

Accumulated Tidal Heating of Stars Over Multiple Pericenter Passages Near SgrA*

Gongjie Li, Abraham Loeb

Institute for Theory & Computation, Harvard-Smithsonian CfA, 60 Garden Street, Cambridge, MA, USA

2 May 2018

ABSTRACT

We consider the long-term tidal heating of a star by the supermassive black hole at the Galactic center, SgrA*. We show that gravitational interaction with background stars leads to a linear growth of the tidal excitation energy with the number of pericenter passages near SgrA*. The accumulated heat deposited by excitation of modes within the star over many pericenter passages can lead to a runaway disruption of the star at a pericenter distance that is 4-5 times farther than the standard tidal disruption radius. The accumulated heating may explain the lack of massive ($\gtrsim 10M_{\odot}$) S-stars closer than several tens of AU from SgrA*.

Key words: black hole physics – galaxies: nuclei – binaries:close – stars: oscillations

1 INTRODUCTION

Near the Galactic center, stars may get scattered into orbits for which the tide raised by the supermassive black hole, SgrA*, at pericenter is large but not strong enough to disrupt the stars. The scattering rate into those orbits is larger than that of immediate tidal disruptions orbits, where the pericenter distances are smaller than the tidal radius, $r_p \lesssim r_t = R_*(M_{\text{BH}}/M_*)^{\frac{1}{3}}$ (Magorrian & Tremaine 1999; Alexander & Livio 2001). Here $M_{\text{BH}} = 4 \times 10^6 M_{\odot}$ is the mass of SgrA* (Ghez et al. 2008; Genzel et al. 2010), and M_* and R_* are the mass and radius of the star. In the near miss regime, stars with $r_p \gtrsim r_t$ are not disrupted during their first passage near SgrA*, their tidal heating and bloating could still be substantial after multiple passages due to the tidal distortion and the excitation of internal oscillation modes. In principle, a sufficiently large number of close passages may lead to the disruption of these stars (Rees 1988; Novikov et al. 1992; Kosovichev & Novikov 1992; Diener et al. 1995; Alexander & Morris 2003; Antonini et al. 2011; Guillochon & Ramirez-Ruiz 2012). Various tidal effects at $r_p \gtrsim r_t$ were considered in the literature, including relativistic effects (Luminet & Marck 1985; Gomboc & Čadež 2005; Ivanov & Chernyakova 2006; Kostić et al. 2009), tidal heating of planets by stars (Ivanov & Papaloizou 2004a, 2007, 2011), and tidal heating in close binary systems (Press & Teukolsky 1977; Kochanek 1992; Mardling 1995a,b; Lai 1997; Ho & Lai 1999; Ivanov & Papaloizou 2004b; Lai & Wu 2006; Fuller & Lai 2011; Weinberg et al. 2012).

In this paper we consider the heating of stars at distances $r_p \gtrsim 3r_t$ from SgrA*. Since each pericen-

ter passage is associated with a small distortion in the shape of stars, one may adopt a linear description for the tidal excitation of stellar modes (Novikov et al. 1992; Kosovichev & Novikov 1992). The associated theory of linear mode excitation has been calibrated recently by new data on stellar binaries from the Kepler satellite (Fuller & Lai 2012; Burkart et al. 2012). The underlying theory was also recently extended to describe nonlinear coupling of the excited modes (Weinberg et al. 2012). We use the latest results from these studies to calculate the tidal excitation and heating of stars in the vicinity of SgrA*.

Our goal is to find the maximum distance from SgrA* at which the accumulated heating due to numerous pericenter passages can lead to tidal disruption of stars around SgrA*. The accumulated heating would lead to the absence of massive stars on eccentric orbits interior to a spherical region around SgrA*, whose radius depends on M_* and exceeds the standard tidal disruption radius r_t . Our predictions could be tested by future searches for stars at closer separations than the known S-stars, which have $r_p \gtrsim 10^2$ AU (Ghez et al. 2008; Genzel et al. 2010).

SgrA* is surrounded by a circumnuclear disk of young stars (Genzel et al. 2010). Inside the inner radius of this disk, there is the S-cluster of young main sequence B-stars (Ghez et al. 2003; Eisenhauer et al. 2005), with random orbital orientations and high orbital eccentricities (Gillessen et al. 2009). All the known S-stars have $r_p \gg r_t$, but it is possible that the lack of S-stars inside 100 AU is caused by the accumulated tidal heating over multiple pericenter passages. Our predictions can be tested as new stars, such as SO-102 (Meyer et al. 2012), are being discovered and new instruments, such as the second-generation VLTI

instrument GRAVITY (Bartko et al. 2009), are being constructed.

The outline of the paper is as follows. In §2 we describe the method we use to calculate the heating due to tidal excitation and the response of the stars. In §3 we show examples of these effects in the Galactic center using two stellar models produced by MESA stellar evolution code (Paxton et al. 2011) and present the results. In §4, we summarize our main conclusions.

2 HEATING OF STARS BY TIDAL EXCITATION OF MODES

The tidal force from SgrA* can excite internal oscillation modes within an orbiting star during its pericenter passages. At distances $r_p \gtrsim 3r_t$, the energy gain by tidal excitation per pericenter passage is low, but the accumulated energy after many passages can heat the star significantly.

2.1 Mode Excitation and Interference in Multiple Pericenter Passages

To calculate the low energy gain per orbit at $r_p \gtrsim 3r_t$, it is appropriate to use the linear perturbation formalism of Press & Teukolsky (1977) (see also Novikov et al. 1992; Kosovichev & Novikov 1992). We denote the separation of the star from SgrA* at time t by $r(t)$. For a single passage, the energy of an excited stellar mode can be expressed as,

$$\Delta E_{0,nml} = 2\pi^2 \left(\frac{GM_*^2}{R_*} \right) \left(\frac{M_{\text{BH}}}{M_*} \right)^2 \left(\frac{R_*}{r_p} \right)^{2l+2} |Q_{nl}|^2 |K_{nlm}|^2, \quad (1)$$

where n is the mode order and $\{l, m\}$ are the two spherical harmonic indices. The excited modes have $l > 1$, $-l < m < l$, and we adopt the convention in which $n < 0$ for g-modes and $n > 0$ for p-modes. The coefficient K_{nlm} represents the coupling to the orbit,

$$K_{nlm} = \frac{W_{lm}}{2\pi} \int_{-\infty}^{\infty} dt \left(\frac{r_p}{r(t)} \right)^{l+1} \exp\{i[\omega_n t + m\Phi(t)]\}, \quad (2)$$

where ω_n is the mode frequency, $\Phi(t)$ is the true anomaly, and $W_{lm} = (-1)^{(l+m)/2} \left[\frac{4\pi}{(2l+1)} (l-m)!(l+m)! \right]^{1/2} / \left[2^l \frac{(l-m)!}{2} \frac{(l+m)!}{2} \right]$. The ‘tidal overlap integral’ Q_{nl} represents the coupling of the tidal potential to a given mode,

$$Q_{nl} = \int_0^1 R^2 dR \rho(R) l R^{l-1} [\xi_{nl}^{\mathcal{R}} + (l+1)\xi_{nl}^{\mathcal{S}}]. \quad (3)$$

where $\rho(R)$ is the stellar density profile as a function of radius R . $\xi(R) = [\xi_{nl}^{\mathcal{R}}(R)\hat{e}_R + \xi_{nl}^{\mathcal{S}}(R)R\nabla]Y_{lm}(\theta, \phi)$ is the mode eigenfunction, with $\xi_{nl}^{\mathcal{R}}$ being its radial component and $\xi_{nl}^{\mathcal{S}}$ being its the poloidal component. The total energy transferred from the orbit to the star in a single passage is

$$\Delta E_0 = \sum_{nlm} \Delta E_{0,nml}. \quad (4)$$

Next, we consider the evolution of the modes as a result of multiple pericenter passages. If the dissipation timescale of the modes is longer than the orbital period, the modes remain excited and interfere with newly excited modes during subsequent passages. Mardling (1995a,b) considered this

problem numerically and found two orbital parameter regions. In one of them the energy exchange between the mode and the orbits is quasi-periodic and the amplitudes of the modes remain small. In the other region, chaotic behavior is exhibited. Ivanov & Papaloizou (2004b) (hereafter IP04) further explored this stability boundary using a proxy α , which characterizes the change of the phase due to the orbital period change, where the period change is caused by the energy transferred to the modes. By mapping the mode amplitude and phase of a particular passage to those values at an earlier passage, IP04 found that when α is larger than a threshold value α_c , there is a secular increase of mode energy. α_c depends on the phase of the mode in the first passage.

For Galactic center stars with $r_p \gtrsim 3r_t$ around SgrA*, the change in orbital period per passage provided by the exchange between tidal excitation energy and orbital energy is too small to increase the mode amplitude. Below we show that gravitational scattering on stars and compact objects in the Galactic center could naturally lead to a drift in the orbital period that allows the amplitude of the excited modes to increase stochastically.

Similar to IP04, we introduce the two-dimensional vectors \mathbf{x}_i to characterize the amplitude A_i and the phase ψ_i of the excited modes at the i^{th} passage:

$$\begin{aligned} x_i^1 &= A_i \cos(\psi_i), \\ x_i^2 &= A_i \sin(\psi_i). \end{aligned} \quad (5)$$

Because different stellar modes act independently in the linear regime, we focus here on one mode with frequency ω_n . For the $(i+1)^{\text{th}}$ passage,

$$\mathbf{x}_{i+1} = \mathcal{R}(\phi_i)[\mathbf{x}_i + \mathbf{e}], \quad (6)$$

where $\phi_i = \omega_n P_{orb,i}$ (with $P_{orb,i}$ being the orbital period for the i^{th} passage), $e^1 = 1$, $e^2 = 0$ and \mathcal{R} is the rotation matrix.

Defining $\alpha_i = \omega_n \Delta P_{orb,i}$ where $\Delta P_{orb,i}$ is the change in the orbital period in the i^{th} passage, we get $\phi_{i+1} = \phi_i + \alpha_i$. In difference from IP04, α_i is a random variable. Given the initial condition $\mathbf{x}_0 = (1, 0)$ (without loss of generality) and equation (6), we examine numerically how the mode amplitude changes as a function of the number of passages. First, we examined the case when α is drawn from a uniform distribution between $-2\alpha_m$ to $2\alpha_m$, $\langle |\alpha| \rangle = \alpha_m$. We characterize the growth in the mode amplitude by the power-law index of its evolution with the number of passages (using a total of 10^6 passages). Figure 1 shows that for $\langle |\alpha| \rangle > 0.1$ the amplitude increases with a power-law index of 0.5, so the energy of the mode increases linearly with time. We also examined an alternative case with α drawn from a Poisson distribution and the result was the same.

Note that in difference from IP04, the increase in the amplitude is caused by the stochastic nature of α . We also find that the threshold value does not show any dependence on ϕ_0 .

Next we examine the value of $\langle |\alpha| \rangle$ due to gravitational perturbers in the Galactic center. We start by expressing α in terms of the fractional change in the orbital period assuming the primary excited mode has frequency $\omega_n \sim$

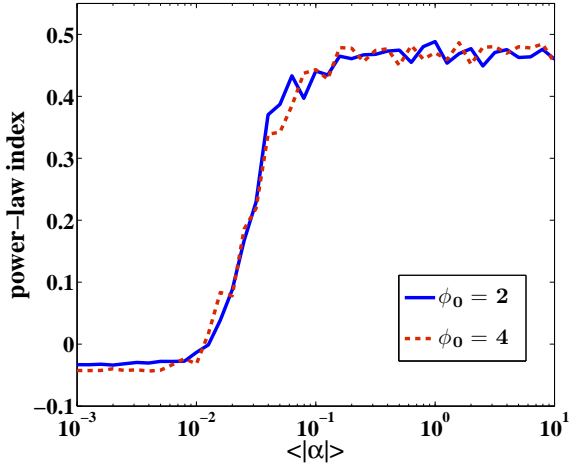


Figure 1. The power-law index of the mode amplitude growth with time during multiple passages as a function of the average magnitude of $\alpha = \omega_n \Delta P_{orb}$. When the power-law index is around 0.5, the amplitude growth resembles a random walk and the energy of the mode is growing linearly with the number of passages. We find this scaling when $\langle |\alpha| \rangle > 0.1$, independent of the value of $\phi_0 = \omega_n P_{orb,0}$ (shown by the different lines).

$$\sqrt{N_{pm} GM_* / R_*^3} \text{ (with a typical value } N_{pm} \sim 10),$$

$$\alpha = \omega_n \Delta P_{orb} \sim 3300 \frac{\Delta P_{orb}}{P_{orb}} \left[\sqrt{\frac{N_{pm}}{10}} \left(\frac{1-0.9}{1-e} \right)^{3/2} \left(\frac{r_p/r_t}{3} \right)^{3/2} \right], \quad (7)$$

where e is the orbital eccentricity. Thus, when $\frac{|\Delta P_{orb}|}{P_{orb}} \gtrsim 3 \times 10^{-5}$ the amplitude of the modes increases stochastically.

We calculate the expected $|\Delta P_{orb}|/P_{orb}$ due to gravitational scatterings using the N-body code BHINT (Löckmann & Baumgardt 2008) to track the orbits of the stars and compact objects in the Galactic center. We estimate $|\Delta P_{orb}|/P_{orb}$ for each passage, and the expectation value is calculated by averaging $|\Delta P_{orb}|/P_{orb}$ over ~ 50 passages. We performed a convergence test and verified that our numerical errors are small and the results are robust. The fractional change in the orbital period of a test star depends on the semi-major axis a and eccentricity e of its orbit and the distribution of perturbers within the S-cluster. We assume an outer radius of ~ 0.04 pc ($= 1''$) for the S-cluster, and estimate the period change for typical S-stars with eccentricities in the range of 0.85–0.95. We consider the initial mass function (IMF) that matches the mass distribution of S-stars inside $0.8''$ ($dN/dm \propto m^{-2.15 \pm 0.3}$) (Bartko et al. 2010)). The fractional change of the orbital period is most sensitive to the massive stars (Murray-Clay & Loeb 2011). We normalize the IMF so that it gives ~ 3 S-stars with $M \sim 20M_\odot$ as observed. In the mass range of $0.3\text{--}25M_\odot$, the IMF yields a total of 800 stars.

We also considered the effects of scattering on stellar-mass black holes (SBH) and a hypothetical intermediate-mass black hole (IMBH). SBHs are more massive than the background stars and therefore are expected to segregate in the Galactic center (Morris 1993; Miralda-Escudé & Gould 2000; Freitag et al. 2006). We normalize the number of

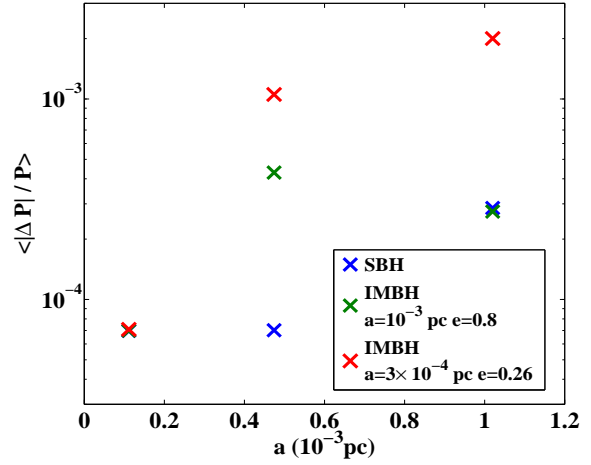


Figure 2. The average of the fractional change in orbital period per pericenter passage, $\langle \Delta P_{orb} / P_{orb} \rangle$, for stars on orbits with different semi-major axis a . The x-axis is in unit of 10^{-3} pc = 206 AU. We include 800 stars with an initial mass function ($dN_*/dM_* \propto M_*^{-2.15}$) (Bartko et al. 2010) in the mass range $0.3\text{--}25M_\odot$, providing about three $20M_\odot$ stars. We also consider scattering on a population of 1,400 stellar-mass black holes (SBH) within 0.04 pc from Sgr A* (Miralda-Escudé & Gould 2000; Freitag et al. 2006), or an intermediate mass black hole (IMBH) with a mass of $10^3 M_\odot$ on two possible orbits.

SBHs (each having $10M_\odot$) within 0.04 pc to be 1400, based on Miralda-Escudé & Gould (2000) and Freitag et al. (2006). An IMBH was hypothesized as an agent for randomizing the inclinations of stars in the S-cluster, potentially creating the hyper-velocity stars and the stellar disk (Yu & Tremaine 2003; Sesana et al. 2006; Yu et al. 2007; Gualandris & Merritt 2009; Perets & Gualandris 2010; Yu 2010). To gauge its effect on ΔP_{orb} we assume an IMBH mass of $10^3 M_\odot$ (Yu 2010) with either $a = 10^{-3}$ pc ($= 206$ AU) and $e = 0.80$ or $a = 3 \times 10^{-4}$ pc and $e = 0.26$. The scattering due to the SBH and IMBH dominate the fractional change in the orbital periods.

Figure 2 shows the results from the numerical runs of the N-body code. We find that the fractional changes of the orbital period are higher than the minimum value required to increase the mode amplitudes stochastically, implying that the energy of the excited modes would increase linearly with the number of pericenter passages. Because the scattering of the orbit is fully random and the change of the orbit is typically small ($\sim 10^{-4}\text{--}10^{-3}$), we neglect the orbital evolution. For a random walk, the period is expected to change significantly only after $10^6\text{--}10^8$ passages, beyond the number of passages considered here.

2.2 Tidal Heating of Stars

Since the expected fractional change in the orbital period per pericenter passage in Figure 2 is higher than 3×10^{-5} , the tidally-excited mode energy is expected to increase linearly with the number of pericenter passages. Cumulatively, a significant amount of heat might be deposited inside the star during multiple passages. In this section, we consider

the dissipation of the mode energy and the resultant heating of the star.

Previous studies showed that when the amplitude of the excited modes increases over some parametric instability threshold, the excited mode begins to transfer its energy to lower frequency daughter modes which dissipate rapidly (Dziembowski 1982; Kumar & Goodman 1996; Wu & Goldreich 2001; Arras et al. 2003; Weinberg & Quataert 2008; Weinberg et al. 2012). We set $n_{crit} = E_{th}/\Delta E_0$ to be the number of pericenter passages after which the amplitude of the mode exceeds this threshold, where E_{th} is the threshold energy when non-linear coupling occurs. As the dissipation time of the excited daughter modes is typically short compared with the orbital period in the Galactic center, the thermal energy gain in the stellar interior is:

$$E_{t,n_p} = (n_p/n_{crit})E_{th} = n_p\Delta E_0, \quad (8)$$

where E_t is the thermal energy gained during this process, n_p is the number of pericenter passages and ΔE_0 is the energy gain of the excited modes during the first passage. When $n_p \gg n_{crit}$, the thermal energy added to the star is independent of the parametric instability threshold.

The heat generated around a radius R within the star at time t_0 will be trapped inside the star for a finite time, $(t - t_0) < t_c(R)$, where $t_c(R)$ is the characteristic time it takes heat to leak out. We estimate $t_c(R)$ as the minimum between the photon diffusion time, $t_{diff} = \int dR\{\tau(R) - (R_* - R)[d\tau(R)/dR]\}/c$, and the turbulent convection time, $t_t = \int dR/v_c(R)$, for each spherical shell inside the star. Here $\tau(R)$ is the scattering optical depth and $v_c(R)$ is the convective velocity. At late times $t > t_c(R)$, the heating at radius R will saturate and reach a steady state where it is balanced by cooling. This sets the upper limit of the maximum heat stored at a radius R .

As the non-linear coupling excites a large number ($> 10^3$) of daughter modes, most of the energy is redistributed. Typically, the daughter modes consist of high order g-modes and so the energy is redistributed mostly in the radiative zone. Weinberg et al. (2012) investigated modes inside solar-type stars and found that most of the energy is transferred to the radiative core of the star. For simplicity, we will assume that the energy is uniformly distributed per unit mass within the radiative zone.

The energy gained can be expressed as follows,

$$E_t(R) = \begin{cases} n_{crit}\Delta E_0(R) & \text{if } t_c(R) < P_{orb}n_{crit} \\ \frac{t_c(R)}{P_{orb}}\Delta E_0(R) & \text{if } t_c(R) > P_{orb}n_{crit} \end{cases} \quad (9)$$

Assuming that energy is evenly deposited throughout the entire radiative zone of the star, we find $E_0(R)$ and obtain the thermal energy stored at a radius R , $E_t(R)$. Typically for stars at $r_p \gtrsim 3r_t$ around SgrA*, $n_{crit} \ll t_c(R)/P_{orb}$, and so the total stored heat is independent of n_{crit} . Finally, integrating $E_t(r)$ over the interior of the star yields the total heating inside the star, E_H .

As a result of the additional source of energy, the star expands. So far, we did not include the increase of the size of the star in our calculation. As the stellar radius increases, the tidal effects become stronger with $\Delta E \propto R_*^6$. A decrease in the mode frequency $\sim \sqrt{GM_*/R_*^3}$ brings ω_n closer to the orbital frequency and increases K_{nl} . Thus, ignoring the

variation in the tidal overlap integral (Q_{nl}), the tidal excitation becomes stronger as the size of the star increases. In addition, the rate of the expansion and the final size of the star depend on where the heat is deposited (Podsiadlowski 1996). We examine this process more closely with MESA stellar evolution simulations (Paxton et al. 2011) in the next section.

As the star gains energy, its energy gain rate increases due to its increasing size. The resulting runaway process could lead to the disruption of the star. In order to find the minimum heating at saturation ($t > t_c(R = 0)$) that may lead to disruption, we express the radius of the star after the n^{th} pericenter passage as, $R_*(n) = R_{*,0}(1 + \epsilon_n)$, where $R_{*,0}$ is the original radius of the star. Assuming $\Delta E \propto R_*(n)^6$ and ignoring the change in entropy within the star, we find

$$1/(1 + \epsilon_n) - 1/(1 + \epsilon_{n+1}) = \Delta\tilde{E}_0((1 + \epsilon_n)^6 - 1), \quad (10)$$

where $\Delta\tilde{E}_0 = \Delta E_0/(GM_*^2/R_{*,0})$. Figure 3 shows the growth of $R_*(n)$ as a function of the number of pericenter passages starting with the saturation value of $\epsilon_0 = 0.01$. Our results demonstrate that at $r_p/r_t \sim 4$ the stored heat can approach the binding energy of the star after $\sim 10^6$ pericenter passages following saturation, even if the total heat gained at saturation is only $\sim 1\%$ of the binding energy. This threshold increases as r_p/r_t increases.

During its lifetime, a massive star can achieve $\gtrsim 10^7$ pericenter passages at the corresponding distances from SgrA*. For example, a $20 M_\odot$ star with $e = 0.9$ and $r_p \sim 5r_t$ around SgrA* has an orbital period of ~ 0.8 years. Thus, during its lifetime the star encounters $\sim 10^7$ pericenter passages. The maximum number of pericenter passages is also limited by gravitational scatterings on other stars. According to Figure 2, with stochastic scatterings on SBH or one hypothesized IMBH, the maximum number of passages at the original pericenter is $\sim 10^6 - 10^8$. Thus, for $r_p/r_t < 5$, the star will be significantly heated even if the total heat gained at saturation is only $\sim 1\%$ of the binding energy.

Non-linear effects are expected to dominate in the last phase of the disruption process. When the star is distorted, the energy transfer from the orbit to the modes can be either positive or negative depending on the phases of the modes and the orientation of the ellipsoid at the time of the pericenter passage. Diener et al. (1995) studied this effect statistically and found that the probability of a positive transfer of energy from the orbit to the star is high.

3 RESULTS

Based on the formalism presented in §2, we calculated the tidal heating of stars in the Galactic center. We consider two stellar masses: $1M_\odot$ (representing low-mass stars) and $20M_\odot$ (representing high mass stars, similar to SO-2 (Martins et al. 2008)). The other properties of the two stars are summarized in Table 1.

Since the energy gain in each passage depends on $(R_*/r_p)^{2l+2}$, and because the value of Q_{nl} and K_{nlm} are similar for modes with different values of l , the quadrupole ($l = 2$) modes gain the most energy during the tidal excitation (whereas $l = 0$ and $l = 1$ modes are not excited). Thus, we focus on the $l = 2$ modes.

We calculate the overlap integral (Q_{nl}) and the

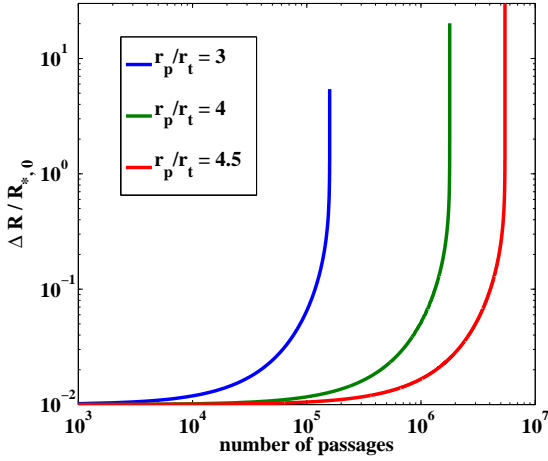


Figure 3. Radius of the star as a function of the number of passages after saturation when $t > t_c(R = 0)$, assuming $\Delta R/R_{*,0}(n = 0) = 0.01$. We find that a star can be heated significantly after $\sim 10^6$ passages even if the thermal energy it stores at saturation is only 1% of its binding energy. This threshold increases as r_p/r_t increases.

Table 1. Properties of stellar models

Mass (M_\odot)	Metallicity	Radius (R_\odot)	Age (yrs)
1	$Z = Z_\odot$	1	4.5×10^9
20	$Z = Z_\odot$	10	7×10^6

orbit coupling (K_{nlm}) using the MESA stellar model (Paxton et al. 2011). The adiabatic normal modes are computed with the ADIPLS code (Christensen-Dalsgaard 2008). For illustration, we show in Figure 4 the values of $\sum_m |Q_{n,l=2}|^2 |K_{n,l=2,m}|^2$ for a $20M_\odot$ star in orbit around Sgr A* with $a = 7 \times 10^{-3}$ pc and $e = 0.9$. As expected (e.g. Press & Teukolsky 1977; Burkart et al. 2012), we find that lower order g-modes are excited the most. The energy gain in one passage, ΔE_0 , can then be found from equation (4).

To calculate the time it takes for the deposited heat to travel to the surface (t_c) as described in §2.2, we obtain the optical depth and the convective velocity profile in the interior of the stars from the MESA code (Paxton et al. 2011). Figure 5 shows the cooling time as a function of radius for the two stars.

The threshold for non-linear coupling has been discussed by Weinberg et al. (2012) for three mode coupling in a solar-mass star. If the daughter modes only couple to one other daughter mode, the threshold is $E_{th} \sim 10^{-19} GM_*^2/R_*$; however, if the daughter modes couple to multiple daughters, $E_{th} \sim 10^{-16} GM_*^2/R_*$. In both cases, $(t_c/t_{orb}) \gg n_{crit}$ in the interior of the stars for $r_p \gtrsim 3r_t$. Thus, the heating of the star is independent of the value of n_{crit} . Conservatively, we calculate the heating using the high energy threshold.

As the daughter modes consist of high order g-modes, energy is redistributed mostly in the radiative zone of the

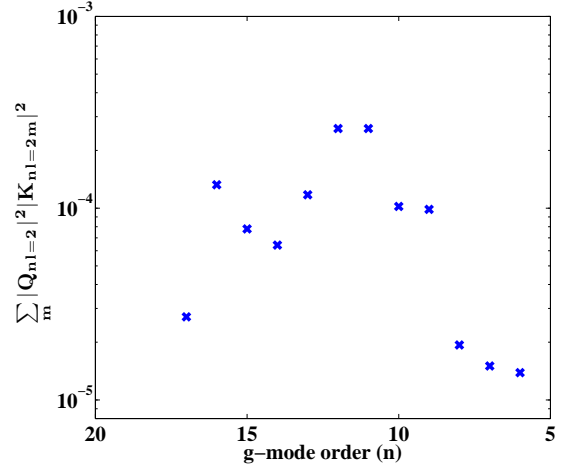


Figure 4. $\sum_m |Q_{n,l=2}|^2 |K_{n,l=2,m}|^2$ as a function of the mode order (n) for stellar modes computed with the ADIPLS code (Christensen-Dalsgaard 2008) based on the stellar structure from the MESA stellar model (Paxton et al. 2011). The mass ($20M_\odot$) and radius ($10R_\odot$) of the star resemble those of SO-2 (Martins et al. 2008).

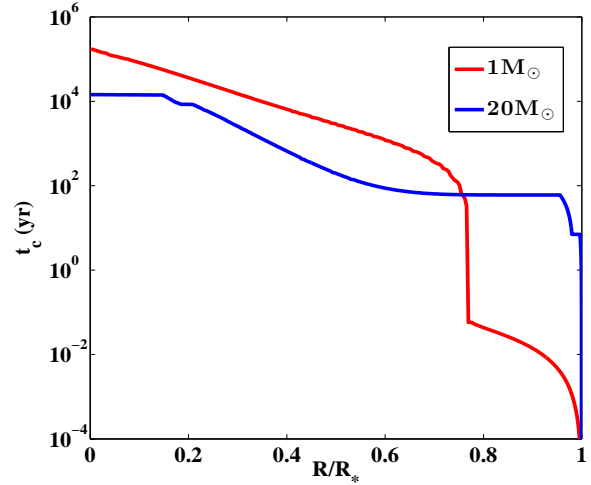


Figure 5. The cooling time (t_c) as a function of radius for the two stars in Table 1.

star. For simplicity, we assume that the distribution is uniform per unit mass in the radiative zone and integrate equation (9) over the interior of the star. Figure 6 shows the heat gained by the stars (E_H) in units of their binding energy (E_B) obtained from MESA, at the saturation time $t = t_c(R = 0)$. The increase in the stellar radius is not included in this calculation.

Taking account of the runaway increase in the stellar radius, the net heat deposited could approach the binding energy and hence lead to disruption when the heating at saturation approaches 1% of the binding energy. We estimate that the heating could be substantial at $r_p \sim 4.5r_t$ for $20M_\odot$ stars.

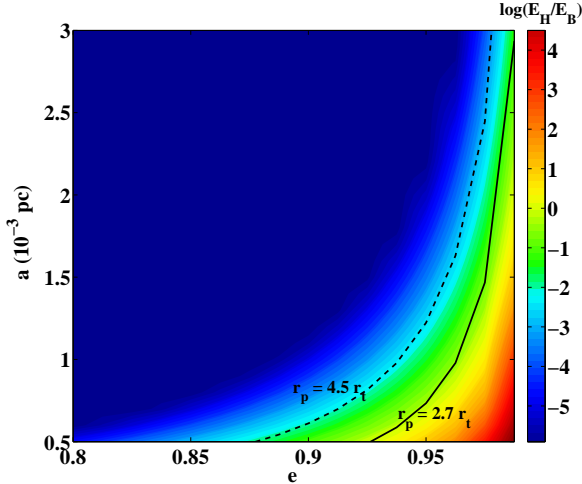


Figure 6. Maximum amount of heat gained at saturation in units of the binding energy of the star as a function of its orbital parameters a and e for a $20M_{\odot}$ star. The solid black line indicates the pericenter distance boundary $r_p = 2.7r_t$ below which the linear tidal excitation formalism is not applicable (Novikov et al. 1992). The dashed black line delineates the threshold $E_H/E_B \sim 0.01$, beyond which the star can potentially be disrupted in $\lesssim 10^6$ pericenter passages. We find that $20M_{\odot}$ stars are significantly heated at $r_p \sim 4.5r_t$.

Next we analyse the heating effect more accurately using MESA stellar evolution simulations. We estimate the heating rate by $\Delta E_0/P_{orb}$, and assume that the heat is deposited uniformly in the radiative zone. We take account of the change in $|Q_{nl=2}|^2|K_{nl=2m}|^2$ due to the change of the stellar structure through iterations. For our first iteration, we assume a constant $|Q_{nl=2}|^2|K_{nl=2m}|^2$ and obtain the structure of the heated stars with different radii at different times. Then we calculate the increase in $|Q_{nl=2}|^2|K_{nl=2m}|^2$ as a function of the increase in stellar radius for the heated stars. For our second iteration, we simulate the heated stars with a changing $|Q_{nl=2}|^2|K_{nl=2m}|^2$ as a function of stellar radius. We calculate $|Q_{nl=2}|^2|K_{nl=2m}|^2$ and continue iterating until the dependence of $|Q_{nl=2}|^2|K_{nl=2m}|^2$ on radius converges. In the examples we consider, convergence is reached within two iterations.

Our convergent results for the $20 M_{\odot}$ star indicate that the size of the convective core decreases and the central temperature stays approximately constant during the heating. For the $1 M_{\odot}$ star, the size of the radiative core increases and the central temperature drops significantly. Figure 7 shows the radius of the heated star as a function of time. We compare the results of the two iterations for the $20 M_{\odot}$ star at $r_p/r_t = 4.5$ and for the $1 M_{\odot}$ star at $r_p/r_t = 5$, and find that the disruption time depends only weakly on the change in $|Q_{nl=2}|^2|K_{nl=2m}|^2$. For other pericenter distances we show only the results of the first iteration (assuming $|Q_{nl=2}|^2|K_{nl=2m}|^2 = \text{const}$). Requiring the heating timescale to be shorter than the orbital scattering timescale and the stellar lifetime, we find that the maximum r_p for disruption is $\sim 4.5r_t$ for a $20 M_{\odot}$ star and $\sim 5r_t$ for a $1 M_{\odot}$ star.

For simplicity, we only considered non-rotating stars. As

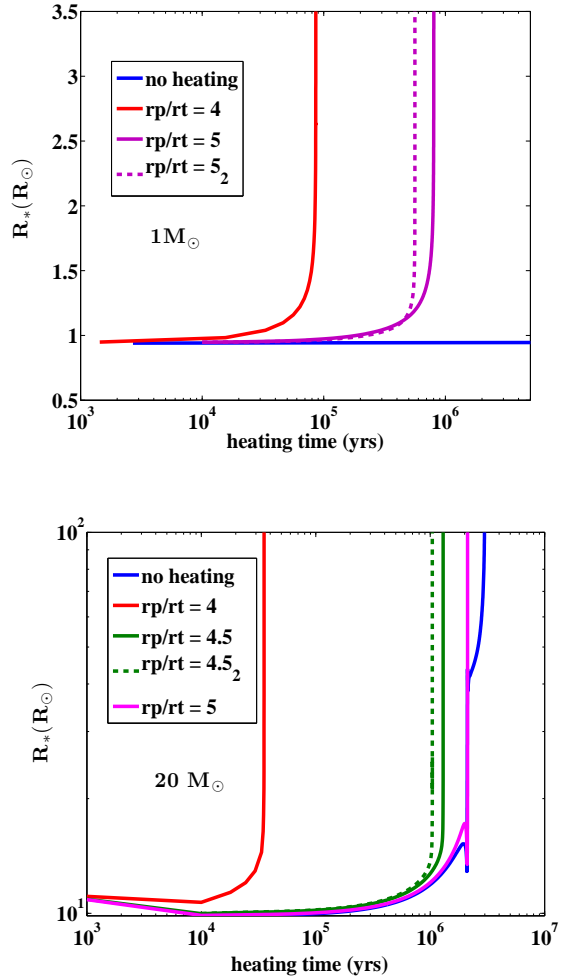


Figure 7. Stellar radius versus heating time. *Top panel:* $1M_{\odot}$ star; *Bottom panel:* $20M_{\odot}$ star. Blue lines indicate the radius change by stellar evolution. Requiring the heating time to be shorter than the orbital scattering timescale ($\sim 10^6$ yrs) and the lifetime of the unheated stars, the maximum r_p for which the stellar radius significantly is $\sim 4.5r_t$ for the $20 M_{\odot}$ star, and $\sim 5r_t$ for the $1 M_{\odot}$ star. At these limiting cases, the dashed lines show results from a second iteration in which $|Q_{nl=2}|^2|K_{nl=2m}|^2$ is updated as the stellar radius increases.

discussed by Fuller & Lai (2012), the mode frequencies are modified for rotating stars by $mC_{nl}\Omega_*$, where Ω_* is the rotation rate of the star and $C_{nl} = \int_0^{R_*} \rho R^2 (2\xi^{\mathcal{R}} \xi^{\mathcal{S}} + \xi^{\mathcal{S}2}) dR$. Because Q_{nl} are unchanged by rotation, the dominant modes shift to higher order g-modes which have smaller values of Q_{nl} . Thus, rotation would lower the excitation energies. In addition, the rotation may modify the modes themselves (Burkart et al. 2012), and further complicate the calculation. Treatment of tidal excitation in misaligned spin-orbit systems were discussed by Ho & Lai (1999) and Lai & Wu (2006).

Finally, we discuss the observational signature of a tidally heated star. Using the MESA simulation, we plot the Hertzsprung-Russell (HR) diagram of the heated stars in Figure 8. Because our calculation is not appropriate in

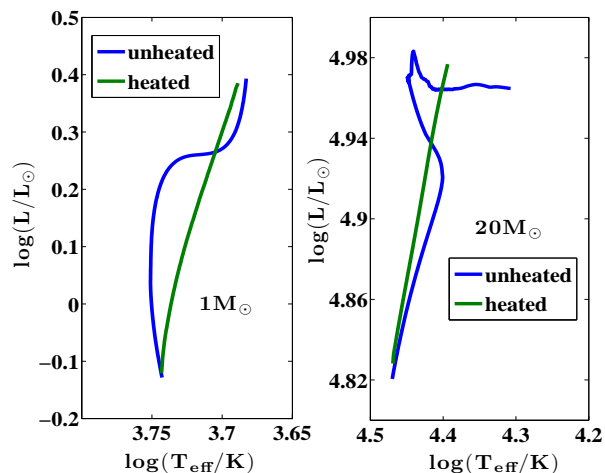


Figure 8. HR diagram of heated stars with masses of $1M_{\odot}$ (left panel) and $20M_{\odot}$ (right panel). Blue lines indicate the evolution track of giant stars with the same masses as they evolve off the main sequence. The HR diagrams of the heated stars stop at the point when the tidal radii of the heated stars approach ($r_p/2.7$), at which point the linear tidal excitation approach breaks down.

the non-linear regime when the tidal radius of the heated star approaches $\sim (r_p/2.7)$, we stop the calculation when $r_p \sim 2.7r_{t,heated}$, where $r_{t,heated}$ is the tidal radius of the heated star. We find that a $1 M_{\odot}$ star at $r_p \sim 2.7r_{t,heated}$ acquires a luminosity L that is ~ 3 times higher than if it were on the main sequence and an effective temperature T_{eff} that is $\sim 12\%$ lower than the main sequence star. A $20M_{\odot}$ star at $r_p \sim 2.7r_{t,heated}$ acquires a luminosity that is $\sim 44\%$ times higher and an effective temperature that is $\sim 20\%$ lower than that on the main sequence. Photometrically, the heated stars could be confused with giant stars that evolved off the main sequence (illustrated by the blue lines in the plot).

4 CONCLUSIONS

We considered the tidal excitation of oscillation modes in stars orbiting SgrA*. When the dissipation timescale of the modes is longer than the orbital period, the modes excited in each passage interfere. Due to the gravitational scatterings on nearby stars or stellar-mass black holes, the orbital period of the excited star changes stochastically and the energy of the excited modes increases approximately linearly with the number of pericenter passages. As non-linear coupling of the stellar modes dissipate the kinetic energy of the modes, the excited star is heated. Once the deposited heat is significant, the star bloats and its tidal heating accelerates, until non-linearities lead to the final mass loss and possible disruption of the star.

We calculated the thermal energy gain by a star as a function of the semi-major axis and eccentricity of its orbit around Sgr A*. We have found that the maximum pericenter distance where the heat gained by the star approaches its binding energy is $r_p \sim 5r_t$ (~ 3.7 AU) for a $1 M_{\odot}$ star and $r_p \sim 4.5r_t$ (~ 13 AU) for a $20 M_{\odot}$ star. The accumulated

heating may explain the lack of massive ($\gtrsim 10M_{\odot}$) S-stars closer than several tens of AU from SgrA* (Genzel et al. 2010).

The heating process may be most effective for the highest-mass stars ($\gtrsim 100M_{\odot}$), where radiation pressure nearly balances gravity and reduces the binding energy considerably relative to GM_*^2/R_* (Shapiro & Teukolsky 1986). This makes these stars more vulnerable to disruption through heating. However, the heating is not important for giant stars evolved off the main sequence, because for $r_p/r_t \sim 5$ the orbital period of a giant star is too long to allow sufficient number of pericenter passages during the star’s lifetime.

The expected radius of the cavity produced by tidal disruption of stars depends on stellar mass (Alexander & Livio 2001). Since gravitational scatterings on other objects could change the orbital period on a timescale much shorter than the lifetime of a low mass star but similar to the lifetime of the high mass star ($\sim 20M_{\odot}$), the net number of pericenter passages is similar in the two cases. Of course, the tidal distance of a high mass star is larger than that of a low mass star, and so a lower mass star may approach Sgr A* at a closer distance (having a shorter orbital time and more pericenter passages) before being tidally disrupted.

The removal of tidally-heated stars makes it more difficult to test the no hair theorem of general relativity based on stellar orbits, as the precession produced by the quadrupole moment of SgrA* decreases with increasing distance. For example, the precession rate due to the quadrupole moment of SgrA* is only $\sim 0.4\mu\text{as/yr}$ for a $20M_{\odot}$ star with $r_p = 4.5r_t$, and is $\sim 4\mu\text{as/yr}$ for a $1M_{\odot}$ star with $r_p = 5r_t$, assuming a normalized spin of 0.7 for SgrA* (Will 2008). Gravitational deflections by other stars or compact objects contaminate the precession signal and require the monitored stars to be within $\sim 2 \times 10^{-4}$ pc from SgrA* (Merritt et al. 2010). We find that only low mass stars (which cannot be detected at present) would be viable targets for testing the no hair theorem around SgrA*.

As new stars, such as SO102 (Meyer et al. 2012), are being discovered in the Galactic center, our predictions for the tidal cavity radius as a function of stellar mass may be tested. In particular, the second-generation VLTI instrument GRAVITY will be able to resolve faint stars with a K-band magnitude $m_K = 18$ ($\sim 3M_{\odot}$) (Bartko et al. 2009) and test our predictions in the coming years.

ACKNOWLEDGMENTS

We thank Charlie Conroy, James Fuller, Bence Kocsis, Leo Meyer, Sterl Phinney, Eliot Quataert and Nick Stone for helpful comments. GL benefitted significantly from the MESA 2012 summer school. This work was supported in part by NSF grant AST-0907890 and NASA grants NNX08AL43G and NNA09DB30A.

REFERENCES

- Alexander T., Livio M., 2001, ApJL, 560, L143
- Alexander T., Morris M., 2003, ApJL, 590, L25

- Antonini F., Lombardi Jr. J. C., Merritt D., 2011, *ApJ*, 731, 128
- Arras P., Flanagan E. E., Morsink S. M., Schenk A. K., Teukolsky S. A., Wasserman I., 2003, *ApJ*, 591, 1129
- Bartko H., Martins F., Trippe S., et al. 2010, *ApJ*, 708, 834
- Bartko H., Perrin G., Brandner W., et al. 2009, *New Astron. Rev*, 53, 301
- Burkert J., Quataert E., Arras P., Weinberg N. N., 2012, *MNRAS*, 421, 983
- Christensen-Dalsgaard J., 2008, *Ap&SS*, 316, 113
- Diener P., Kosovichev A. G., Kotok E. V., Novikov I. D., Pethick C. J., 1995, *MNRAS*, 275, 498
- Dziembowski W., 1982, *Acta Astron*, 32, 147
- Eisenhauer F., Genzel R., Alexander T., et al. 2005, *ApJ*, 628, 246
- Freitag M., Amaro-Seoane P., Kalogera V., 2006, *ApJ*, 649, 91
- Fuller J., Lai D., 2011, *MNRAS*, 412, 1331
- Fuller J., Lai D., 2012, *MNRAS*, 420, 3126
- Genzel R., Eisenhauer F., Gillessen S., 2010, *Reviews of Modern Physics*, 82, 3121
- Ghez A. M., Duchêne G., Matthews K., Hornstein S. D., Tanner A., Larkin J., Morris M., Becklin E. E., Salim S., Kremenek T., Thompson D., Soifer B. T., Neugebauer G., McLean I., 2003, *ApJL*, 586, L127
- Ghez A. M., Salim S., Weinberg N. N., Lu J. R., Do T., Dunn J. K., Matthews K., Morris M. R., Yelda S., Becklin E. E., Kremenek T., Milosavljevic M., Naiman J., 2008, *ApJ*, 689, 1044
- Gillessen S., Eisenhauer F., Trippe S., Alexander T., Genzel R., Martins F., Ott T., 2009, *ApJ*, 692, 1075
- Gomboc A., Čadež A., 2005, *ApJ*, 625, 278
- Gualandris A., Merritt D., 2009, *ApJ*, 705, 361
- Guillochon J., Ramirez-Ruiz E., 2012, *ArXiv e-prints*
- Ho W. C. G., Lai D., 1999, *MNRAS*, 308, 153
- Ivanov P. B., Chernyakova M. A., 2006, *AAP*, 448, 843
- Ivanov P. B., Papaloizou J. C. B., 2004a, *MNRAS*, 353, 1161
- Ivanov P. B., Papaloizou J. C. B., 2004b, *MNRAS*, 347, 437
- Ivanov P. B., Papaloizou J. C. B., 2007, *MNRAS*, 376, 682
- Ivanov P. B., Papaloizou J. C. B., 2011, *Celestial Mechanics and Dynamical Astronomy*, 111, 51
- Kochanek C. S., 1992, *ApJ*, 385, 604
- Kosovichev A. G., Novikov I. D., 1992, *MNRAS*, 258, 715
- Kostić U., Čadež A., Calvani M., Gomboc A., 2009, *AAP*, 496, 307
- Kumar P., Goodman J., 1996, *ApJ*, 466, 946
- Lai D., 1997, *ApJ*, 490, 847
- Lai D., Wu Y., 2006, *PRD*, 74, 024007
- Löckmann U., Baumgardt H., 2008, *MNRAS*, 384, 323
- Luminet J.-P., Marck J.-A., 1985, *MNRAS*, 212, 57
- Magorrian J., Tremaine S., 1999, *MNRAS*, 309, 447
- Mardling R. A., 1995a, *ApJ*, 450, 722
- Mardling R. A., 1995b, *ApJ*, 450, 732
- Martins F., Gillessen S., Eisenhauer F., Genzel R., Ott T., Trippe S., 2008, *ApJL*, 672, L119
- Merritt D., Alexander T., Mikkola S., Will C. M., 2010, *PRD*, 81, 062002
- Meyer L., Ghez A. M., Schoedel R., Yelda S., Boehle A., Lu J. R., Do T., Morris M. R., Becklin E. E., Matthews K., 2012, submitted to *Science*
- Miralda-Escudé J., Gould A., 2000, *ApJ*, 545, 847
- Morris M., 1993, *ApJ*, 408, 496
- Murray-Clay R. A., Loeb A., 2011, *ArXiv e-prints*
- Novikov I. D., Pethick C. J., Polnarev A. G., 1992, *MNRAS*, 255, 276
- Paxton B., Bildsten L., Dotter A., Herwig F., Lesaffre P., Timmes F., 2011, *ApJS*, 192, 3
- Perets H. B., Gualandris A., 2010, *ApJ*, 719, 220
- Podsiadlowski P., 1996, *MNRAS*, 279, 1104
- Press W. H., Teukolsky S. A., 1977, *ApJ*, 213, 183
- Rees M. J., 1988, *Nature*, 333, 523
- Sesana A., Haardt F., Madau P., 2006, *ApJ*, 651, 392
- Shapiro S. L., Teukolsky S. A., 1986, *Black Holes, White Dwarfs and Neutron Stars: The Physics of Compact Objects*
- Weinberg N. N., Arras P., Quataert E., Burkert J., 2012, *ApJ*, 751, 136
- Weinberg N. N., Quataert E., 2008, *MNRAS*, 387, L64
- Will C. M., 2008, *ApJL*, 674, L25
- Wu Y., Goldreich P., 2001, *ApJ*, 546, 469
- Yu Q., 2010, in *Dynamics from the Galactic Center to the Milky Way Halo Limits on a black hole companion to SgrA**
- Yu Q., Lu Y., Lin D. N. C., 2007, *ApJ*, 666, 919
- Yu Q., Tremaine S., 2003, *ApJ*, 599, 1129